Femtosecond-laser-written, stress-induced $Nd:YVO_4$ waveguides preserving fluorescence and Raman gain

W. F. Silva,[1,*] C. Jacinto,[1] A. Benayas,[2] J. R. Vazquez de Aldana,[3] G. A. Torchia,[4] F. Chen,[5] Y. Tan,[5] and D. Jaque[2]

[1]*Grupo de Fotônica e Fluidos Complexos, Instituto de Física, Universidade Federal de Alagoas, 57072-970, Maceió, Alagoas, Brazil*

[2]*Departamento de Física de Materiales, Facultad de Ciencias, Universidad Autónoma de Madrid, Madrid 28049, Spain*

[3]*Grupo de Optica, Facultad de Ciencias, Universidad de Salamanca, Salamanca 37008, Spain*

[4]*CIOp, Centro de Investigaciones Ópticas, CIC-Conicet, CC 124, La Plata 1900, Argentina*

[5]*School of Physics, Shandong University, Jinan 250100, China*

[*]*Corresponding author: wagner@fis.ufal.br*

Received December 7, 2009; revised February 2, 2010; accepted February 4, 2010; posted February 25, 2010 (Doc. ID 121032); published March 18, 2010

We report the formation of optical waveguides in the self-Raman $Nd:YVO_4$ laser crystal by femtosecond laser inscription. The confocal fluorescence and Raman images have revealed that the waveguide is constituted by a locally compressed area in which the original fluorescence and Raman gains of the $Nd:YVO_4$ system are preserved. Thus the obtained structures emerge as promising candidates for highly efficient self-Raman integrated laser sources. © 2010 Optical Society of America

OCIS codes: 160.0160, 160.5690, 140.0140, 140.3330.

Neodymium-doped yttrium orthovanadate (hereafter $Nd:YVO_4$) is nowadays a paradigm among solid-state lasers [1]. It simultaneously combines the outstanding spectroscopic properties of Nd^{3+} ions in the YVO_4 lattice (broad absorption bands and high absorption and emission cross sections) [2] with the excellent properties of the YVO_4 host (good thermal and mechanical properties and high Raman gain) [3], making this material especially suitable for the fabrication of highly efficient diode-pumped self-Raman lasers [4]. Different techniques have been used so far to produce waveguide structures in $Nd:YVO_4$, mainly ion implantation and Nd^{3+} ion in-diffusion [5,6]. Unfortunately, these methods have inherent drawbacks, such as the absence of true 3D design and the deterioration of the Nd^{3+} fluorescence properties [7]. Thus the search for a versatile microstructuring method for the fabrication of 3D $Nd:YVO_4$ waveguides preserving its original features is still open.

Femtosecond laser inscription has been demonstrated to be a very powerful technique for the fabrication of waveguides with controlled properties via the adequate choice of the inscription parameters [8]. Despite the good results obtained in other laser systems [9–11], the possibility of waveguide fabrication in $Nd:YVO_4$ crystals by femtosecond laser inscription has not been yet explored.

In this Letter we report, for the first time to our knowledge, on the fabrication of channel-buried optical waveguides in a $Nd:YVO_4$ crystal by femtosecond laser inscription showing both TM and TE confinements. We also have used confocal micro-fluorescence and micro-Raman images of the fabricated structures to evaluate the spatial location, magnitude, and nature of the microstructural and refractive index changes induced in the $Nd:YVO_4$ network.

The $Nd:YVO_4$ (1 at.% doped) crystal used in this work is a plate with sizes of $6\times2\times5$ mm^3 along the a, b, and c axes, respectively. The buried waveguide was fabricated by using an amplified Ti:sapphire laser system providing 120 fs pulses linearly polarized at 796 nm with 1 kHz repetition rate. The laser beam, propagating along the c axis of the $Nd:YVO_4$ crystal, was focused with a 10× microscope objective (NA=0.3), and the translation of the sample (along the a crystallographic direction) was achieved by a 0.2 μm resolution motorized stage. The linear focus of the objective was located at 250 μm below surface, and two laser tracks were written separated 15 μm by translating the sample with a speed of 50 μm/s (five times higher than previously used in femtosecond laser inscription of Nd:YAG waveguides) [11]. The writing-pulse energy was varied from 10 up to 25 μJ obtaining the best results (in terms of waveguiding properties) from an intermediate energy of 13 μJ/pulse. Figure 1(a) shows a microscope optical transmission image of the waveguide's end face obtained with this optimum energy. The relative orientation of the crystallographic axes is schematically

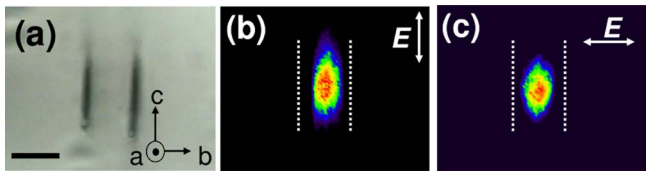

Fig. 1. (Color online) (a) Optical micrograph of the waveguide's cross section. Near-field distributions of waveguide's mode obtained at 632.8 nm with a polarization (b) parallel and (c) perpendicular to the damage tracks. The scale bar is 15 μm for the three pictures. The location of the damage tracks is systematically indicated by the dashed lines.

indicated. The near-field intensity distributions at 632.8 nm of the waveguide's modes obtained for TE and TM polarizations are shown in Figs. 1(b) and 1(c). The isotropic waveguiding suggests that both the ordinary and extraordinary refractive indexes have been increased in the region between filaments. This is an advantage over recently reported femtosecond-laser-written stress-induced Nd:YAG waveguides, which showed confinement only for a single polarization [11]. The waveguide's propagating losses were estimated (by using the Fabry–Perot method at 632.8 nm [12]) to be as low as 0.8 dB/cm, comparable with other waveguides in which efficient laser action has been demonstrated [9].

The microluminescence and microstructural characterization of the waveguide's cross section was performed by using an Olympus BX-41 fiber-coupled confocal microscope equipped with a 50× objective and a 488 nm argon laser, as described elsewhere [7]. Figure 2(a) shows the ${}^4F_{3/2} \rightarrow {}^4I_{11/2}$ μ-PL (photoluminescence) spectra obtained when the 488 nm beam was focused at an unmodified zone (bulk), at one of the damage tracks and at the waveguide. For these spectra it is clear that the Nd^{3+} fluorescence intensity is well preserved at waveguide's volume, being reduced only at the damage tracks [see the spatial variation of the Nd^{3+} fluorescence intensity in Fig. 2(b)]. Figure 2(c) shows the spatial variation of the spectral position of the laser transition (main fluorescence peak located at around 9400 cm^{-1}). It is clear

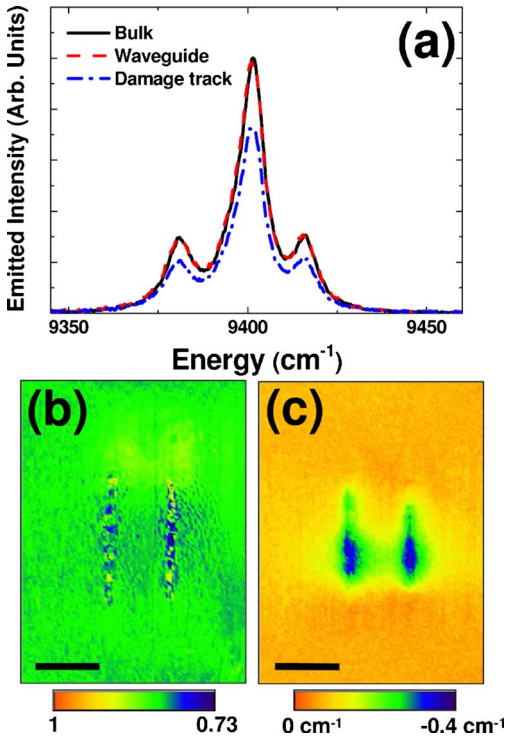

Fig. 2. (Color online) (a) ${}^4F_{3/2} \rightarrow {}^4I_{11/2}$ μ-PL spectra obtained from the unmodified $Nd:YVO_4$ area (bulk), from a damage track and from the waveguide. (b) Spatial distribution of the ${}^4F_{3/2} \rightarrow {}^4I_{11/2}$ fluorescence intensity. (c) Spatial map of the induced shift in the main fluorescence peak within the ${}^4F_{3/2} \rightarrow {}^4I_{11/2}$ emission band. Scale bars are, in all cases, 15 μm.

from Fig. 2(c) that the main laser line has been shifted to lower energies at the damage tracks and between them (i.e., at waveguide). This induced redshift (as large as -0.4 cm^{-1} and -0.2 cm^{-1} at the damage tracks and the waveguide, respectively) can be attributed, according to previous works, to a local compression of the YVO_4 network [13]. Based on the previously reported pressure coefficient of this laser line (approximately -4.57 cm^{-1}/GPa), it is now possible to estimate the residual stress induced in the YVO_4 lattice at waveguide's location, to be $R_{stress} \sim 44$ MPa. This residual compressive stress leads to a volume reduction of $\Delta V/V = -3\ R_{stress}/E_{YVO} \sim -1 \times 10^{-3}$, where $E_{YVO} \approx 133$ GPa is the YVO_4 Young's Modulus. Assuming, in a first-order approximation, that lattice compression is the main mechanism leading to refractive index modification, it is now possible to estimate the refractive index increment induced at the waveguide's location based on the Claussius Mossoti expression, which leads to $\Delta n \approx 1.5 \times 10^{-3}$ [3]. This value, which well explains the appearance of a waveguide, can be compared with those previously reported for other waveguides whose origin is the volume change induced in the proximities of ultrafast written tracks such as sapphire crystals ($\Delta n \approx 1 \times 10^{-4}$) [14], Nd:YAG ceramics ($\Delta n \approx 5 \times 10^{-3}$) [15], and LiTaO crystals ($\Delta n \approx 10^{-4}$) [16]. Of course, the contribution of other mechanisms, such as changes in the electronic polarizability and slight compositional changes, cannot be disregarded at this point.

Figure 3 summarizes the results obtained from the μ-Raman experiments. In Fig. 3(a) we show a detail of the μ-Raman spectra obtained from the waveguide, from an unperturbed area and from the damage track. Note that only at the damage track there is an appreciable drop in the Raman efficiency. This indeed accounts for the presence of defects [as already postulated from the analysis of the fluorescence maps of Fig. 2(b)]. Indeed, the Raman intensity image of Fig. 3(b) indicates that the fabricated waveguides will keep the characteristic high Raman gain of the $Nd:YVO_4$ system, making the obtained waveguides promising candidates for the development of integrated self-Raman laser sources. Finally, Fig. 3(c) shows the spatial distribution of the energy position of the Raman mode shown in Fig. 3(a) (around 888 cm^{-1}). This Raman mode experiences a blueshift at the damage tracks and in the spatial region delimited by them. Since this Raman mode is known to shift to higher vibration energies when compressive stresses are applied, the Raman image of Fig. 3(c) supports the previous conclusion extracted from the fluorescence images; a local compression of the $Nd:YVO_4$ network has been produced at the damage tracks and in the region between them. Furthermore, from the induced shift and the pressure coefficient of the analyzed Raman mode (+0.25 cm^{-1} and 6.5 cm^{-1}/GPa [17], respectively) we have estimated a residual compressive stress of 38 MPa, in excellent agreement with that determined from the fluorescence images of Fig. 2.

In summary, we have fabricated buried channel waveguides in the $Nd:YVO_4$ self-Raman laser sys-

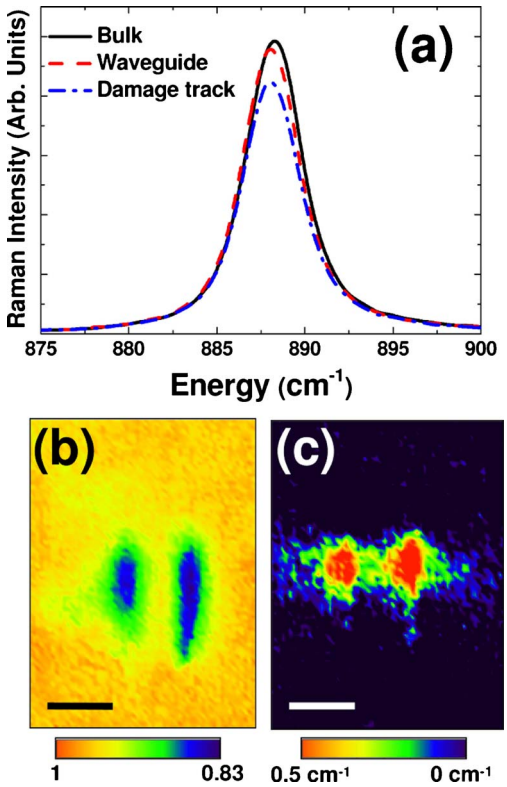

Fig. 3. (Color online) (a) Detail of the μ-Raman spectra obtained from the unmodified Nd:YVO_4 area (bulk), from a damage track and from the waveguide. (b) Spatial distribution of the Raman intensity. (c) Spatial map of the induced shift in the main most-intense Raman peak (888 cm^{-1} Raman mode). Scale bars are, in all the cases, 15 μm.

tem by ultrafast laser inscription of damage tracks. The obtained waveguides have shown polarization-independent light confinement with propagation losses as low as 1 dB/cm. The confocal fluorescence and Raman images have been used to establish that femtosecond laser inscription has produced a local lattice compression at damage tracks and between them, which we believe is the origin of the waveguide formation. First-order calculations have estimated a refractive index increment at waveguide's location of the order of 10^{-3}. Finally, we have found, from the analysis of the confocal microfluorescence and micro-Raman images, that both the Nd^{3+} fluorescence and YVO_4 Raman efficiencies are well preserved at the waveguide's volume. Thus the fabricated structures emerge as promising candidates for the future development of integrated self-Raman lasers.

This work has been supported by the Spanish Ministerio de Ciencia y Tecnología (MAT2007-64686, CSD2007-00013), and FIS2009-09522) the UAM-CAM (CCG08-UAM/MAT-4434), Conicet (Argentina) under project PIP (11220090100394), the National Natural Science Foundation of China (NSFC) (10925524), CEAL-Banco Santander, and Brazilian agencies CAPES and CNPq.

References

1. A. A. Kaminskii, *Laser Crystals: Their Physics and Properties* (Springer, 1990).
2. T. Taira, A. Mukai, Y. Nozawa, and T. Kobayashi, Opt. Lett. **16**, 1955 (1991).
3. J. L. Blows, T. Omatsu, J. Dawes, H. Pask, and M. Tateda, IEEE Photonics Technol. Lett. **10**, 1727 (1998).
4. H. Zhu, Y. Duan, G. Zhang, C. Huang Y. Wei W. Chen, Y. Huang, and N. Ye, Opt. Lett. **34**, 2763 (2009).
5. F. Chen, L. Wang, Y. Jiang, X. L. Wang, K. M. Wang, G. Fu, Q. M. Lu, C. E. Ruter, and D. Kip, Appl. Phys. Lett. **88**, 071123 (2006).
6. S. J. Hettrick, J. S. Wilkinson, and D. P. Shepherd, J. Opt. Soc. Am. B **19**, 33 (2002).
7. A. Benayas, D. Jaque, S. J. Hettrick, and J. S. Wilkinson, J. Appl. Phys. **103**, 103104 (2008).
8. S. Nolte, M. Will, J. Burghoff, and A. Tuennermann, Appl. Phys. A **77**, 109 (2003).
9. G. A. Torchia, A. Rodenas, A. Benayas, E. Cantelar, L. Roso, and D. Jacque, Appl. Phys. Lett. **92**, 111103 (2008).
10. N. D. Psaila, R. R. Thomson, H. T. Bookey, A. K. Kar, N. Chiodo, R. Osellame, G. Cerullo, A. Jha, and S. Shen, Appl. Phys. Lett. **90**, 131102 (2007).
11. J. Siebenmorgen, K. Petermann, G. Huber, K. Rademaker, S. Nolte, and A. Tünnermann, Appl. Phys. B **97**, 251 (2009).
12. R. Regener and W. Sohler, Appl. Phys. B **36**, 143 (1985).
13. F. J. Manjon, S. Jandl, G. Riou, B. Ferrand, and K. Syassen, Phys. Rev. B **69**, 165121.1 (2004).
14. V. Apostolopoulos, L. Laversenne, T. Colomb, C. Depeursinge, R. P. Salathé, and M. Pollnau, Appl. Phys. Lett. **85**, 1122 (2004).
15. A. Ródenas, G. A. Torchia, G. Lifante, E. Cantelar, J. Lamela, F. Jaque, L. Roso, and D. Jaque, Appl. Phys. B **95**, 85 (2009).
16. B. McMillen, K. P. Chen, H. L. An, S. Fleming, V. Hartwell, and D. Snoke, Appl. Phys. Lett. **93**, 111106.1 (2008).
17. A. Jayaraman, G. A. Kourokouklis, G. P. Espinosa, A. S. Cooper, and L. G. Van Uitert, J. Phys. Chem. Solids **48**, 755 (1987).